Decomposition of Naphthalene by dc Gliding Arc Gas Discharge

6 AUTHORS, INCLUDING:

Liang Yu
General Electric
19 PUBLICATIONS   **181** CITATIONS

SEE PROFILE

Xin Tu
University of Liverpool
58 PUBLICATIONS   **749** CITATIONS

SEE PROFILE

Shengyong Lu
Zhejiang University
136 PUBLICATIONS   **981** CITATIONS

SEE PROFILE

Decomposition of Naphthalene by dc Gliding Arc Gas Discharge

Liang Yu,[†] Xiaodong Li,[†] Xin Tu,[‡] Yu Wang,[†] Shengyong Lu,[†] and Jianhua Yan*,[†]

State Key Laboratory of Clean Energy Utilization, Institute for Thermal Power Engineering, Zhejiang University, Hangzhou 310027, P. R. China, and Center for Surface Chemistry and Catalysis, Katholieke Universiteit Leuven, Heverlee 3001, Belgium

Gliding arc discharge has been proved to be effective in treatment of gas and liquid contaminants. In this study, physical characteristics of dc gliding arc discharge and its application to naphthalene destruction are investigated with different external resistances and carrier gases. The decomposition rate increases with increasing of oxygen concentration and decreases with external resistance. This value can be achieved up to 92.3% at the external resistance of 50 kΩ in the oxygen discharge, while the highest destruction energy efficiency reaches 3.6 g (kW h)$^{-1}$ with the external resistance of 93 kΩ. Possible reaction pathways and degradation mechanisms in the plasma with different gases are proposed by qualitative analysis of postdestructed products. In the air and oxygen gliding arc discharges, the naphthalene degradation is mainly governed by reactions with oxygen-derived radicals.

1. Introduction

Polycyclic aromatic hydrocarbons (PAHs), designated as priority pollutants by the U.S. EPA, have attracted increasing attention due to their carcinogenicity, mutagenicity, and toxicity to mammals.[1,2] Incomplete combustion of fossil fuels and waste incineration can lead to release a mass of PAHs.[3] Many countries have legislated strict laws on emission control because the emission of PAHs in the atmosphere is detrimental to both human beings and the environment. Therefore, it is necessary to develop effective technologies to destruct PAHs from the flue gas.

This work looks specifically at the decomposition of naphthalene, the most common type of PAH, and the major component of the char.[4] In recent years, many works focus on the removal of naphthalene from wastewater and flue gas. Scientists have been developing several types of efficient technologies to decompose naphthalene and other PAHs, including sorbent or surfactant absorption,[5–7] electron beam irradiation,[8] and catalytic oxidation.[9,10] However, each of above means has restrictions. Naphthalene is not destructed but is transmitted from gas or aqueous solution to the surface of sorbent or surfactant by the absorption methods. For the catalytic oxidation, the main concerns are the price of the catalysts, some of which are noble metals, and catalyst poisoning. Naphthalene in flue gas can be treated effectively by electron beam irradiation, but the electron beam generation system and irradiation flow system are complicated. As an alternative approach, nonthermal plasma technology has been utilized for volatile organic compounds (VOCs) remediation for many years.[11–15] Because of the large number of high energy electrons and radicals and relative low gas temperature, nonthermal plasma is regarded as a promising technology for gas phase pollutants destruction. In this study, we study the naphthalene decomposition efficiency by gliding arc discharge, which has

been utilized for abatement of some other gas pollutants and considered as an efficient kind of nonthermal plasma by many scientists.

Gliding arc plasma is an auto-oscillating phenomenon that develops between at least two electrodes.[16,17] When the high voltage power source provides high enough voltage between electrodes, the gas flow between the electrodes gap is broken down and the arc is formed. The arc is then pushed downstream by the gas flow and glides along the electrode surface until it quenches. After the decay of discharge, there is a new breakdown at the narrowest gap and the cycle repeats. This periodical discharge evolves from an arc to a discharge, corresponding to containing both quasi-equilibrium and non-equilibrium phases.[18] Compared to other atmospheric nonthermal plasmas, gliding arc discharge has a special advantage in that it can provide both a high level of power and a high degree of nonequilibrium state, which is the reason it attracts considerable interest for its applications: hydrogen production,[19–21] VOC abatement,[22–25] degradation of wastewater,[26–31] materials surface treatment,[32] etc. A preliminary study of destruction PAHs released from the combustion of polyethylene (PE) and poly-(vinyl chloride) (PVC) by ac gliding arc plasma was carried out by Du et al.[33] However, the naphthalene destruction efficiency and mechanism have not been reported due to the absence of naphthalene in those experiments.

In this study, the effects of initial concentration, carrier gas, and external resistor on the naphthalene destruction process by gliding arc plasma are studied. Different reaction pathways, degradation mechanisms, and roles of active species in the process with various gases are proposed by analysis of decomposition efficiency and products at different operation conditions.

2. Experimental Setup and Analysis Method

The experimental setup (Figure 1) consists of a naphthalene-laden gas generation system, a dc gliding arc plasma system, an off-gas absorption system, and an electrical measurement system. Powdered naphthalene is placed in a glass bottle and heated to 40 °C with a water bath. Naphthalene vapor is carried

* Corresponding author. E-mail: yanjh@zju.edu.cn. Tel.: +86-571-87952443; +86-571-87952438.
† Zhejiang University.
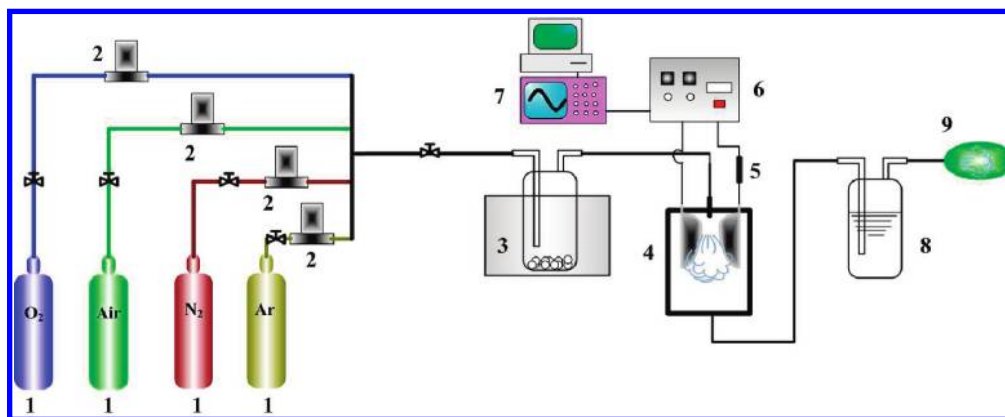‡ Katholieke Universiteit Leuven.

Figure 1. Schematic diagram of the experimental setup: 1, gas source; 2, mass flow controller; 3, water bath; 4, gliding arc reactor; 5, external resistor; 6, dc power supply; 7, digital oscilloscope; 8, absorption bottle; 9, gas bag.

along by a gas flow of 6.8 L min^{-1} and sprayed into the gliding arc plasma reactor. The gliding arc plasma system consists of a dc power supply (0−6150 V, 900 W), an external resistance bank (50−93 kΩ), and a gliding arc reactor. In order to analyze the reaction products, the gas flow passes through an absorption bottle containing hexane. The off-gas is analyzed both qualitatively and quantitatively by a FTIR spectrometer. Each experiment lasts for 3 min. Products dissolved in the absorption solution are analyzed by gas chromatography with mass spectrometric detection (GC/MS). Chromatographic separation is carried out on a 60 m DB-5 silica-fused capillary column with internal diameter 0.25 mm and a stationary phase film thickness of 0.25 μm. The temperature program for the GC oven is initial temperature 70 °C, hold for 5 min; 70−270 at 8 °C min^{-1}; 270 °C, hold for 30 min. Carrier gas: helium, 1 mL min^{-1}; hydrogen, 3.5 mL min^{-1}. Injector and detector temperatures are set to 250 and 280 °C, respectively. Mass spectrometer working condition: electron impact ionization 70 eV, ion source temperature 250 °C. The mass range is selected from 50 to 300 *m/z*. The arc voltage and current intensity are measured synchronously by an oscilloscope (Tektronix TDS2024), a current probe (TCP303/TCPA300), and a high voltage probe (P6015A).

The naphthalene destruction rate η_d, the energy efficiency η_e, and the destruction capacity N_d in this paper are defined as follows:

$$\eta_d = \frac{X_{in} - X_{out}}{X_{in}} \times 100\% \tag{1}$$

$$\eta_e = \frac{(X_{in} - X_{out}) \times f_{gas}}{P_{GA}} \tag{2}$$

$$N_d = (X_{in} - X_{out}) \times f_{gas} \tag{3}$$

where X_{in} is the initial naphthalene concentration, X_{out} is the final naphthalene concentration, f_{gas} is the carrier gas flow rate, and P_{GA} is the power of the gliding arc plasma.

3. Results and Discussion

Electrical Characteristics of dc Gliding Arc Plasma. In this study, physical characteristics of the dc gliding arc plasma are examined at a carrier gas flow rate of 6.8 L min^{-1}, which provides valuable knowledge to get a better understanding of the naphthalene degradation mechanisms.

Figure 2 shows the arc voltage and current signals of the gliding arc plasma for different carrier gases. The electrical signals exhibit periodical oscillation and zigzag shapes when
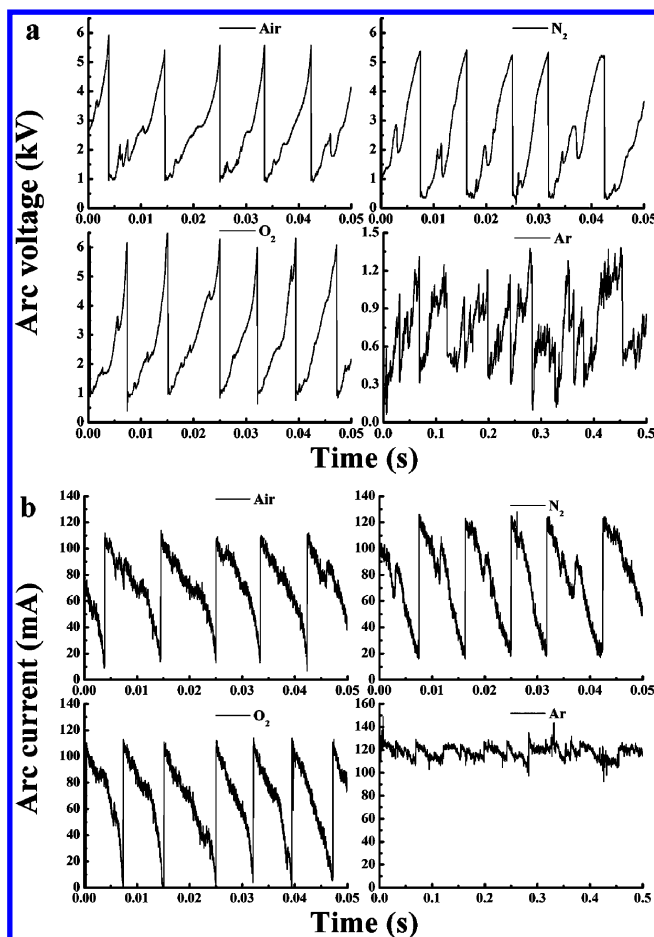

Figure 2. Gliding arc voltage (a) and current (b) waveforms with different carrier gases (external resistance: 50 kΩ).

air, nitrogen, and oxygen are used as carrier gases. As can be observed in Figure 2, after a quasi-linear evolution correlated to the downstream movement of the arc root on the electrode surface, the arc voltage suddenly drops when a breakdown occurs in the electrode gap, followed by an arc quench and the formation of a new arc on the electrode neck. Arc root is arc attachment on the electrode, which is also the joint of arc column and electrode.[34]

The highest arc voltage (the lowest arc current) corresponds to the breakdown voltage (current) of the starting point. The arc voltage variation behavior is contrary to that of arc current. The fluctuation characteristics of gliding arc electrical signals at these operation conditions are consistent with the previous
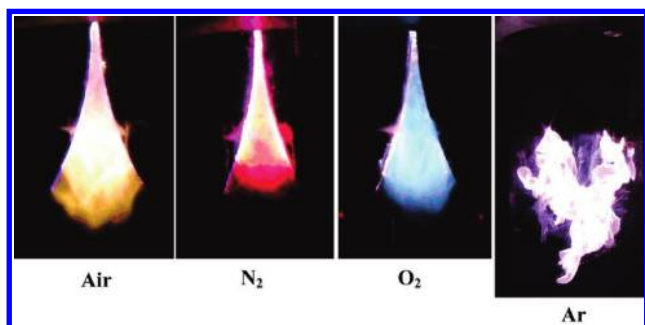
Figure 3. Photos of gliding arc discharge in different carrier gases.

TABLE 1: Average Arc Voltages, Arc Currents, and Periods with Different Carrier Gases and Resistance of 50 kΩ

carrier gas	air	N_2	O_2	Ar
average voltage/kV	2.54	2.37	2.69	0.72
average current /mA	72	76	68.5	118
average period/ms	9.2	9.1	8.2	>500

literature.[35,36] It is worth noting that the electrical signals of argon gliding arc are more irregular than those of other discharges. From the arc voltage waveform of argon discharge, we can find that the arc voltage of argon plasma is much lower compared with that of the discharge in other gases. For the arc current, the fluctuation amplitude (0.118 A) is much lower than that of other kinds of plasma. Such behavior suggests that the argon gliding arc is rarely quenched in these experiments. The argon gliding arc has the lowest breakdown voltage, which results in easy formation and hard extinction of an argon plasma. During our experiments without naphthalene in carrier gases, different plasma structures are observed with various carrier gases, as shown in Figure 3. The appearance of a gliding arc in air, nitrogen, and oxygen can be characterized by the presence of a stable plasma area caused by the periodic arc movement; in argon, however, a white arc is jumping between the electrodes without quenching due to the turbulence of argon gas flow.

Physical parameters, such as average arc voltage, current, and arc lifetime, are presented in Table 1. The oxygen gliding arc has the highest arc voltage, while the argon arc voltage is much lower than that of all others. Therefore, the local electric field strength is relatively low in argon gliding arc plasma. Conversely, the average arc current is the largest in the argon plasma. The carrier gas also presents a significant influence on the average arc current.

Influence of Carrier Gas and External Resistance on Naphthalene Decomposition. In order to study the influence of carrier gas and external resistance on the naphthalene destruction process, experiments with different carrier gases and resistances are now studied. The initial naphthalene concentration, dependent on the water bath temperature and gas flow rate, is about 1.32 mg L^{-1} after a 30 min stabilization without discharge at the gas flow rate of 6.8 L min^{-1} and a water bath temperature of 40 °C.

Figure 4 shows the destruction rates obtained with different carrier gases. Average arc voltages, currents, and power measured in the experiments are shown in Table 2. The naphthalene destruction rate varies from 7.74% to 92.3%, depending on working conditions. In an oxygen gliding arc, the maximum destruction rate (92.3%) can be achieved at an external resistance of 50 kΩ. The destruction rate decreases with rising external resistance, which is ascribed to the prominent influence of arc current and arc power. Decreasing arc current leads to a reduction of arc length and generation of less energetic electrons and active species, which lowers the naphthalene destruction rate in the gliding arc process. Table 2 shows the decreasing trend of arc power and arc current with rising external resistance, which can also lead to the reduction of electron energy and the number of radicals. Arc voltage increases with rising external resistance. Comparing plasma with different gases, the average arc voltages follow an order of oxygen > air > nitrogen > argon, while the average arc currents vary in an opposite order. Table 2 shows that the increasing amplitude of arc current (∼70%) is much higher than decreasing amplitude of arc voltage (∼10%) with the external resistance decreasing from 93 to 50 kΩ, which indicates the arc current is a more dominant contributor to power than voltage. The destruction rate is evidently higher in oxygen than in other gases. From a chemical viewpoint, free radicals generated in discharge are distinct in different gases tested. In the oxygen and air discharge, the species formed such as O and O(^{3}P) have much stronger oxidation ability than the free radicals in nitrogen discharge, which also results in the higher destruction rate in oxygen and air discharge. Table 2 indicates that the arc current in nitrogen discharge is higher than that in oxygen and air, yet the naphthalene destruction rate is lower. This result indicates that in a comparison of different carrier gases the chemical aspect in this process predominates over the physical aspect. The argon gliding arc in these experiments fluctuates and is unsteady, whatever the external resistance selected. Low arc voltage, low arc power, and instability in argon gliding arc are the three major contributors to the low destruction efficiency. On the other handt, the free radicals generated from different types of plasma also play a vital role in the destruction process in various atmospheres. Free radicals, such as O and OH, produced in oxygen gliding arc enhance the naphthalene decomposition. These radicals have much stronger oxidizing ability than those formed in other types of plasma, which explains the highest naphthalene degradation efficiency achieved in an oxygen gliding arc discharge. On the contrary, species generated in argon plasma show less oxidizing power. The process of naphthalene oxidation by radicals in different kinds of plasma is discussed in a later section.

Destruction Energy Efficiency Evaluation. Energy efficiency of naphthalene destruction at different experimental conditions displayed in Figure 5 illustrates the increasing trend of energy efficiency with rising external resistance except when the carrier gas is argon. The highest destruction energy efficiency (3.6 g (kW h)$^{-1}$) is achieved with the external resistance of 93 kΩ and oxygen carrier gas. Fridman et al. divided a gliding arc cycle into a quasi-equilibrium phase and a nonequilibrium phase

TABLE 2: Average Arc Voltages, Arc Currents, and Arc Powers at Different Experimental Conditions

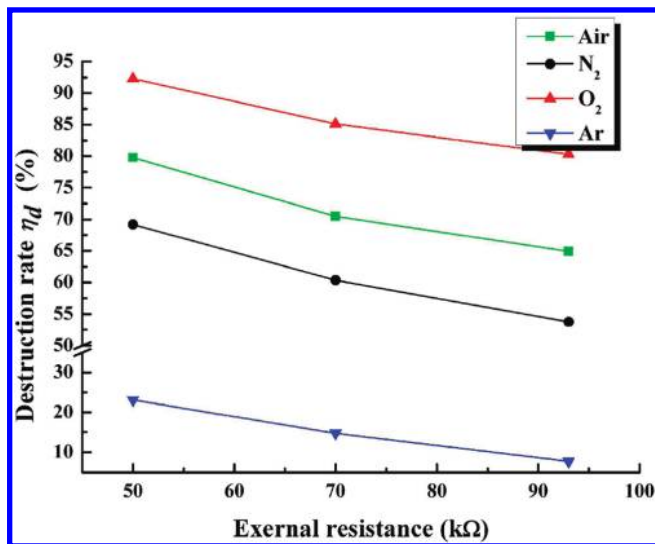| carrier gas	average arc voltage /kV				average arc current /mA				average arc power /W			
	air	N_2	O_2	Ar	air	N_2	O_2	Ar	air	N_2	O_2	Ar
93 kΩ	2.44	1.80	2.67	0.34	50.14	55.13	45.04	64.62	122.3	99.2	120.2	21.97
70 kΩ	2.31	1.67	2.55	0.32	65.93	71.46	56.74	86.55	152.3	119.3	144.6	27.7
50 kΩ	2.20	1.60	2.45	0.30	85.72	95.45	78.05	116.5	188.5	152.7	191.2	34.95

Figure 4. Naphthalene destruction rates at various experimental conditions (naphthalene initial concentration: 1.32 mg L^{-1}).
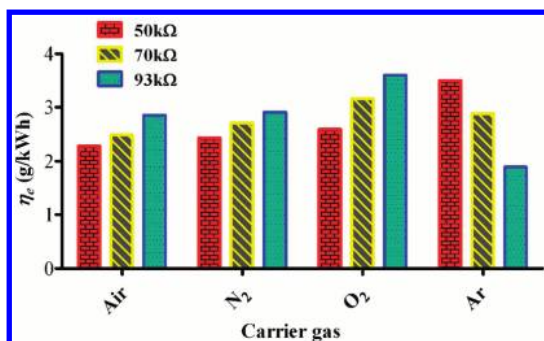

Figure 5. Naphthalene destruction energy efficiencies at various experimental conditions (naphthalene initial concentration:1.32 mg L^{-1}).

by using the critical electrical parameters.[17] Mutaf-Yardimci et al. investigated the effect of the gas flow rate and the external resistance on the gliding arc characteristics.[18] According to the literature, nonequilibrium of the discharge increases with rising external resistance value. Thereby, the destruction energy efficiencies suggest that the most economical decomposition process corresponds to the highest nonequilibrium degree, which is in agreement with the literature.[37] On the contrary, in an argon discharge destruction energy efficiency declines with rising external resistance value. This may be ascribed to the unstable state of discharge, resulting in irregular fluctuations in the plasma electrical parameters so that the degradation energy consumption undulates in a large range. Naphthalene removal from flue gas has been studied in an electron beam plasma reactor where the experimental G-value of 1.66 mol/100 eV was gained at a dose of 1 kGy.[8] Nair et al. have used the pulsed corona discharges to remove tar from biomass-derived flue gas. Naphthalene removal efficiency can be achieved up to 90% at the energy density of 400 J/L.[38]

Influence of Initial Naphthalene Concentration on the Destruction Process. Figure 6 shows that the destruction rate decreases by ~35% and destruction capacity triples when the naphthalene initial concentration increases from 0.75 to 4.75 mg L^{-1}. The lower destruction rate at rising initial naphthalene concentration is due to the availability of fewer electrons and reactive species per naphthalene molecule. At the same time,
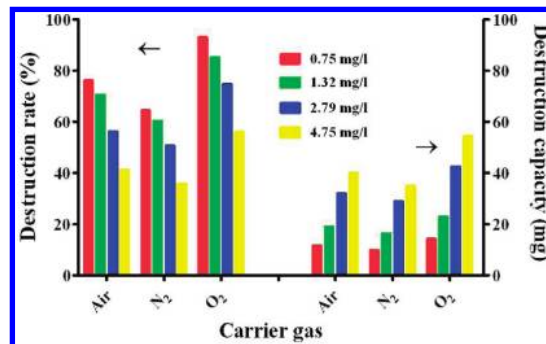

Figure 6. Naphthalene destruction rates and capacities at various initial concentrations (external resistance: 70 kΩ).
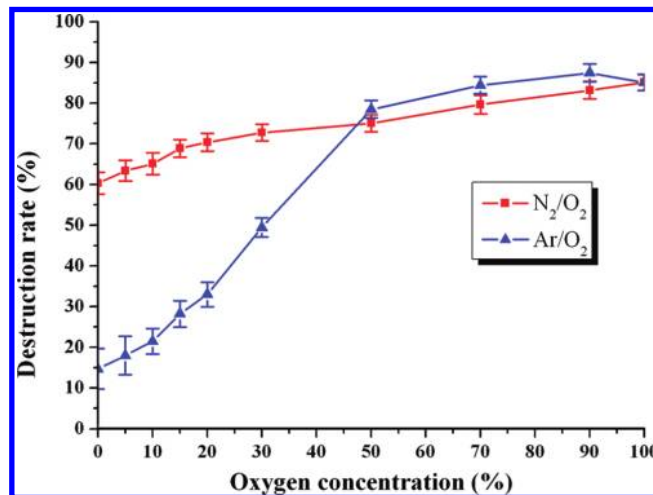

Figure 7. Naphthalene destruction rates at different oxygen concentrations (external resistance, 70 kΩ; naphthalene initial concentration, 1.32 mg L^{-1}).

the relatively high level power in gliding arc plasma guarantees the increasing of naphthalene destruction capacity with rising initial concentration. However, it should be noted that the increasing amplitude of decomposition capacity is about half of that of initial concentration. These results indicate that the gliding arc discharge is a promising technology for abatement of high concentration waste gas.

Naphthalene Destruction in a N$_2$/O$_2$ Mixture and an Ar/O$_2$ Mixture. Naphthalene is swept into the plasma reactor by a N$_2$/O$_2$ mixture and an Ar/O$_2$ mixture, respectively, with variable oxygen concentration. As shown in Figure 7, it is interesting to observe that the decomposition rate in Ar/O$_2$ is lower than that in N$_2$/O$_2$ when the oxygen concentration is lower than 50%. Furthermore, the two curves are very close within the error estimation when the oxygen concentration is greater than 50%. A naphthalene destruction rate up to 87.4% can be achieved at the oxygen concentration of 90%. The average arc voltage and current values for different oxygen concentration displayed in Figure 8 demonstrate some reasons for this interesting influence. The arc voltage in a N$_2$/O$_2$ discharge is much larger than that in an Ar/O$_2$ discharge when the oxygen concentration is lower than 50%. Although the arc current in an Ar/O$_2$ discharge is larger than that in a N$_2$/O$_2$ discharge, the distinction amplitude of arc current is lower than that of arc voltage with the oxygen concentration below 50%. The arc voltages in these two kinds of mixture discharge are almost the same, and the difference of arc currents in two mixture discharge decreases when the oxygen concentration exceeds 50%.

Figure 9 plots the concentration of CO and CO$_2$ in a N$_2$/O$_2$ discharge as a function of oxygen volume fraction. In the curve
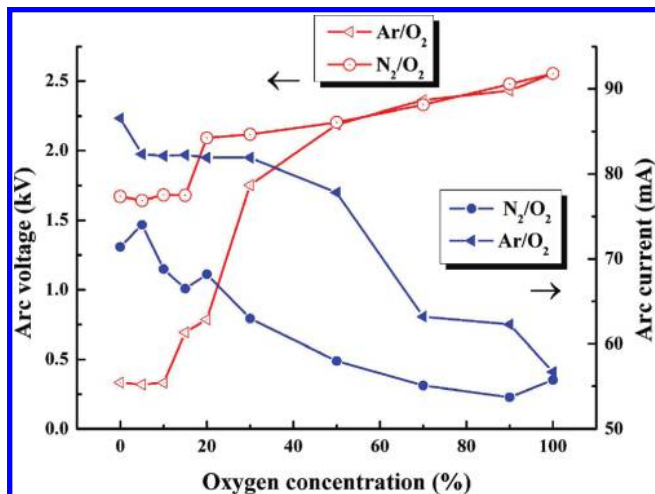
Figure 8. Average arc voltages and arc currents at different oxygen concentrations (external resistance, 70 kΩ; naphthalene initial concentration, 1.32 mg L^{-1}).
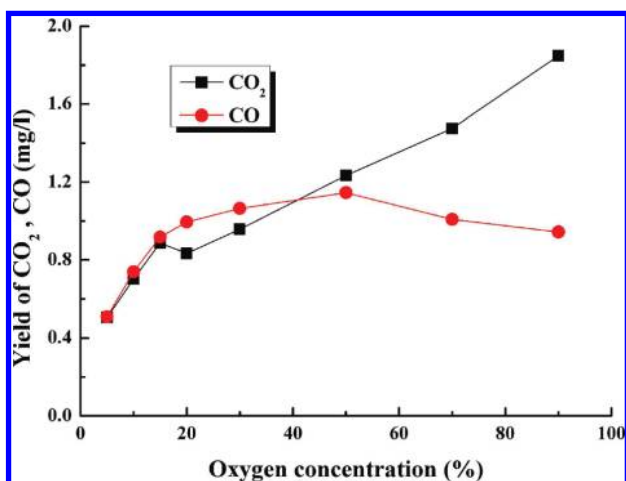

Figure 9. Yields of CO_2 and CO at different oxygen concentrations in N_2/O_2 mixture discharge. External resistance, 70 kΩ; naphthalene initial concentration, 1.32 mg L^{-1}.

of CO an inflection point is found, corresponding to the oxygen concentration of 50%. When the oxygen concentration is higher than 50%, the yield of CO decreases with the rising of oxygen concentration, which indicates that the selectivity of CO also decreases after this oxygen ratio point. In Table 4, it can be seen that the yields of NO and NO_2 decrease when oxygen concentration is larger than 50%. This decreasing trend of NOx formation indicates that the amount of O radicals, which participate in the NOx formation process, decreases when oxygen concentration is more abundant than nitrogen. These results indicate that then more oxygen-derived species such as O, O(^{1}D), O(^{3}P), and O_3 can react with CO to promote the conversion from CO to CO_2 when the oxygen is more than N_2 in the mixture. Figure 10 shows the two distinct variation trends of CO and CO_2 arising in an Ar/O_2 discharge. The yield of CO_2 is continuously increasing with rising O_2 concentration. For CO, two distinct O_2 concentration ranges can be distinguished: from 0 to 50%, CO concentration increases significantly; then, it is approximately constant when the O_2 concentration is larger than 50%. The ratio between the yields CO_2 and CO in an Ar/O_2 mixture discharge increases markedly with rising O_2 concentration. These quite distinct variation trends of the CO and CO_2 concentration in the off-gas indicate that the Ar/O_2 discharge has a higher CO_2 selectivity in the naphthalene decomposition process.
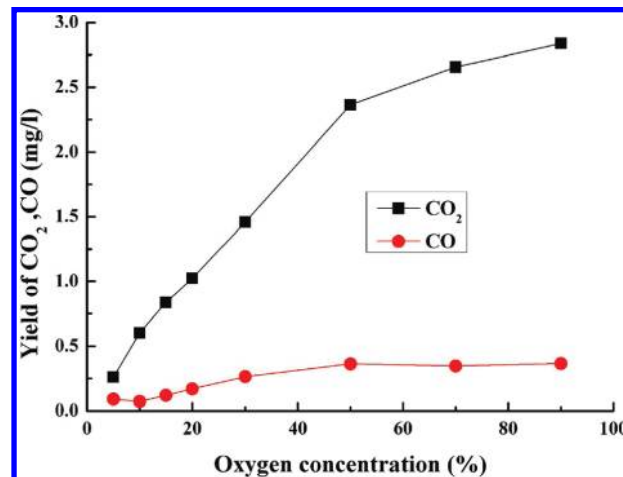

Figure 10. Yields of CO_2 and CO at different oxygen concentrations in Ar/O_2 mixture discharge. External resistance, 70 kΩ; naphthalene initial concentration, 1.32 mg L^{-1}.

TABLE 3: CO and CO_2 Selectivities and Carbon Balance in N_2/O_2 and Ar/O_2 Discharges

	N_2/O_2			Ar/O_2		
	selectivity %		carbon balance %	selectivity %		carbon balance %
O_2 %	CO	CO_2		CO	CO_2	
5	27.8	17.5	45.3	17.3	37.1	49.0
10	39.3	23.8	63.1	11.7	61.9	73.6
15	46.1	28.4	74.5	14.7	65.4	80.2
20	49.0	26.1	75.1	17.7	68.5	86.2
30	50.7	29.0	79.7	18.5	65.1	83.6
50	52.9	36.3	89.2	16.0	66.5	82.5
70	43.9	40.9	84.8	14.2	69.5	83.7
90	39.3	49.0	88.3	14.5	71.7	86.2

The selectivity for the production of CO or CO_2 is defined as follows:

$$S_{CO} = \frac{[CO]}{10 \times [N_d]} \times 100\% \tag{4}$$

$$S_{CO} = \frac{[CO_2]}{10 \times [N_d]} \times 100\% \tag{5}$$

The carbon balance in this paper is given by

$$CB = \frac{C_{CO} + C_{CO_2}}{C_d} \times 100\% \tag{6}$$

where C_{CO} and C_{CO_2} are the moles of carbon of CO and CO_2 measured at the outlet, whereas C_d is the moles of carbon in converted naphthalene. CO and CO_2 selectivities and carbon balance values are listed in Table 3. It can be found that naphthalene presents a larger selectivity for CO generation in the N_2/O_2 mixture discharge and a higher selectivity for CO_2 formation in the Ar/O_2 mixture discharge. Kim et al.[39] reported a major reaction route for a CO_2 production in a discharge via reaction of OH with CO:
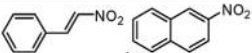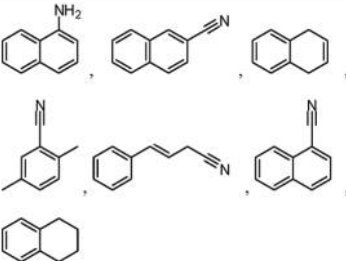
$$CO + OH \rightarrow CO_2 + H \tag{R1}$$
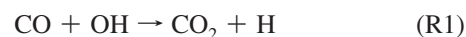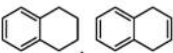
This reaction accounts for a higher CO_2 selectivity in an Ar/O_2 gliding arc than that in a N_2/O_2 discharge. Some OH can be consumed in a N_2/O_2 mixture discharge by some other free radicals and byproducts, such as NO and NO_2. In an Ar/O_2 discharge, relatively fewer species can react with OH. The closure of carbon balance increases with rising oxygen con-

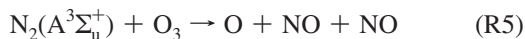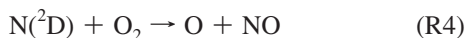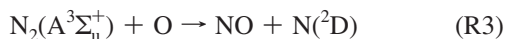**TABLE 4: Yields of NO and NO₂ in Various Oxygen Concentrations**

O_2/N_2	5/95	10/90	15/85	20/80	30/70	50/50	70/30	90/10
O_2 %	5	10	15	20	30	50	70	90
NO mg/L	0.7	2.29	2.59	2.94	2.97	2.75	2.14	1.29
NO_2 mg/L	0.05	0.25	0.34	0.53	0.80	1.08	1.00	0.61
NO/NO_2 (vol %/vol %)	21	14.14	11.44	8.52	5.69	3.89	3.26	3.25

TABLE 5: Compounds Identified in Postdestructed Products

centration, which can be ascribed to a rising CO or CO_2 selectivity. A carbon balance value up to ∼88% and ∼86% can be achieved in two mixture discharge. In our experiments, brown carbon deposition on the reactor inner surface is observed. This phenomenon is more obvious in the low oxygen concentration. The other part of carbon of about 15% exists in brown carbon and some other carbon-containing end products.

Table 4 presents the concentrations of NO and NO_2 in the discharge with a N_2/O_2 mixture as a function of oxygen ratio. The NO concentration (0.7−3 mg/L) is much higher than that of the NO_2 (0.05−1 mg/L). With rising oxygen ratio in carrier gas, the concentration of NO and NO_2 first increases and then decreases. The oxygen ratios corresponding to the maximum concentration of NO and NO_2 are 0.3 and 0.5, respectively. When the oxygen ratio exceeds 0.5, the generation of NO and NO_2 decreases with the rising of oxygen ratio, which is ascribed to the decreasing trend of nitrogen acting as a reagent in the NOx formation process. The basic knowledge of NOx formation in a nonthermal plasma system has been well-established,[39,40] and it includes the following reactions:

$$N(^2P) + O_2 \rightarrow O + NO \quad (R2)$$

$$N_2(A^3\Sigma_u^+) + O \rightarrow NO + N(^2D) \quad (R3)$$

$$N(^2D) + O_2 \rightarrow O + NO \quad (R4)$$

$$N_2(A^3\Sigma_u^+) + O_3 \rightarrow O + NO + NO \quad (R5)$$

$$NO + O_3 \rightarrow O_2 + NO_2 \quad (R6)$$

$$O + NO + M \rightarrow NO_2 + M \quad (R7)$$

The oxygen concentration threshold[39] of 5% in NOx formation is not observed in these experiments. As the oxygen ratio is 5%, the NO and NO_2 attain about 0.7 and 0.05 mg/L,

respectively. Furthermore, the yield of NO is larger than that of NO_2 in the entire oxygen scale, which is distinct from the NOx generation in a ferroelectric pellet packed-bed reactor.[39] This distinction is ascribed to the different plasma and discharge reactor type and relative higher power of plasma in gliding arc. From the previous literature,[40,41] it follows that the largest contributors for the NO formation are $N_2(A^3\Sigma_u^+)$ and $N(^2D)$ but not the electronically exited state of oxygen atoms. Compared with mixture $N_2/O_2 = 1/9$ and $N_2/O_2 = 3/7$ discharges, there are relatively high concentrations of electronically exited nitrogen atoms such as $N_2(A^3\Sigma_u^+)$ and $N(^2D)$ in the mixture $N_2/O_2 = 9/1$ and $N_2/O_2 = 7/3$ discharges, which leads to the higher productions of NO as shown in Table 4. NO_2 is generated via R6 and R7 in discharge. From Table 4, it is obvious that the yield ratio of NO to NO_2 decreases with the increase of oxygen concentration, which indicates that the conversion from NO to NO_2 is promoted by the oxygen increase. This result can be ascribed to the rising trends of O and ozone generation with the increase of oxygen concentration.

As an example, Figure 11 shows a series of chromatograms recorded at various oxygen levels in an Ar/O_2 mixture discharge. Two peaks appear in the chromatograms, and both their amplitudes decrease with oxygen volume fraction increasing from 5% to 30% and then they disappear when the oxygen concentration exceeds 50%. Peak 1 and peak 2 are assigned to 1,2-dihydronaphthalene and 1,2,3,4-tetrahydronaphthalene, respectively, by mass spectrometry detection. On the basis of qualitative analysis of postdestructed mixtures, a possible naphthalene degradation pathway in an Ar/O_2 background gas is suggested. Decomposition is initialized through the dehydrogenation by energetic electron impact, as confirmed by observation of soot formation during these experiments. Subsequently, some stable intermediates such as 1,2-dihydronaphthalene and 1,2,3,4-tetrahydronaphthalene are formed by reaction with H radical. Compared with the naphthalene, these intermediates are more easily oxidized by active species and dissociated by electron collision. Finally, these intermediates are oxidized to final products such as CO and CO_2. This simplified reaction pathway is not the unique channel in the degradation process; however, it is undoubtable that the formation of 1,2-dihydronaphthalene and 1,2,3,4-tetrahydronaphthalene accelerates the conversion from naphthalene to final products. With rising oxygen concentration, the initialization of destruction process via the reactions between O and naphthalene becomes more predominant.

Analysis of the Byproduct in the Naphthalene Decomposition Process. All the identified stable products at different experimental conditions are listed in Table 5. When the background gas is nitrogen, more kinds of products are identified than with other carrier gases. Byproducts at these experimental conditions are classified into four groups: (i) two-ringed compounds with N-containing substituent; (ii) two-ringed compounds without substituent; (iii) one-ringed compounds; (iv) hydrogen cyanide. Based on a qualitative analysis of the offgas, possible decomposition pathways in a nitrogen discharge are proposed. For the high concentration of nitrogen, the excited state of nitrogen can be easily generated in the discharge. Hence,
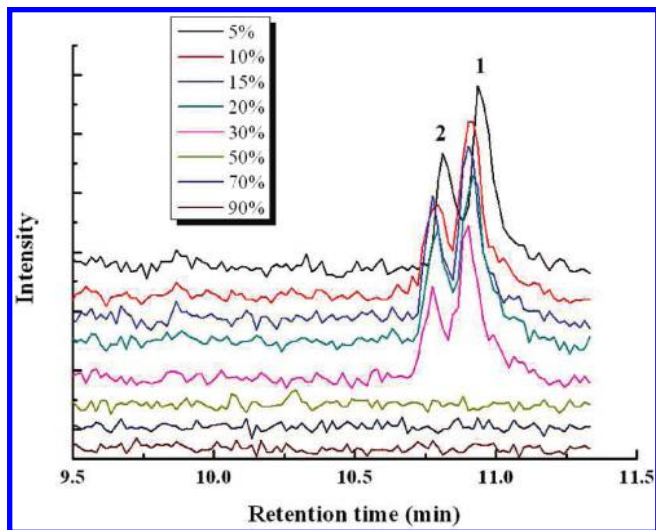
Figure 11. Series of chromatograms recorded in Ar/O$_2$ mixture discharge.

these destruction pathways are mainly initiated via reactions with nitrogen excited states such as N$_2$(A$^3\Sigma_u^+$) and N$_2$(^{2}D):

$$C_{10}H_8 + N_2(A^3\Sigma_u^+) \rightarrow C_{10}H_7 + H + N_2 \qquad (R8)$$

$$C_{10}H_8 + N_2(A^3\Sigma_u^+) \rightarrow C_9H_7 + CH + N_2 \qquad (R9)$$

$$C_{10}H_8 + N_2(^2D) \rightarrow product \qquad (R10)$$

Additionally, high energy electron impact may also participate in reactions.[42–44] However, the electron direct impact is much less predominant than the reactions with nitrogen excited state for the small electron collision cross section of hydrocarbon and low concentration of naphthalene. Although some ions such as N$_2^+$ and N$^+$ were observed by Delair et al.,[45] data concerning the absolute concentrations of these ions are very limited. Therefore, it is very complicated to estimate the ion reactions in the destruction process.

(1) Naphthalene is eliminated by dehydrogenation initiated via R8 and hydrogenation reactions, which leads to the formation of two-ringed compounds without substituents such as tetralin and 1,4-dihydronaphthalene. This dehydrogenation process can be confirmed by the observing carbonization phenomenon during the experiment with the carrier gas of nitrogen: soot is found on the inner surface of the quartz reactor in nitrogen discharge experiments. (2) Naphthalene is decomposed through reactions with hydrogen cyanide and the CN radical, which can be confirmed by the existence of two types of naphthalene substituted compounds, naphthalene-1-carbonitrile and naphthalene-2-carbonitrile, and hydrogen cyanide. Ring cleavage in naphthalene via R9 and in some intermediates produces the CH radical, which acts as a reactant in the hydrogen cyanide and CN radical formation reactions.[46,47]

$$CH + N_2 \rightarrow HCN + N \qquad (R11)$$

$$CH + N \rightarrow CN + H \qquad (R12)$$
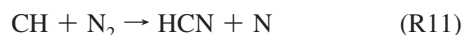
Despite the existence of no data in previous literature concerning the reaction between CN and aromatic hydrocarbons, the existence of naphthalene-1-carbonitrile (C$_{10}$H$_7$−CN) and some other CN-containing compounds indicates that CN radical would recombine with C$_{10}$H$_7$ or other intermediates. Blin-Simiand et al. have also found the possibility of reactions between CN radical and phenyl or between CN and methyl−phenyl in toluene destruction process by DBD discharge.[42]

(3) As a third possible degradation pathway, hydrocarbon rings in naphthalene and some products generated from destruction pathway (1) are directly destroyed by some excited state of nitrogen molecules such as N$_2$(A$^3\Sigma_u^+$) and N$_2$(^{2}D). Then intermediates from these reactions finally react with CN to form stable products such as one-ringed compounds with CN-substituent.
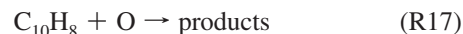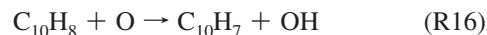
When the naphthalene destruction is carried out in the oxygen gliding arc plasma, the byproducts are distinct from those in the nitrogen discharge. Because of strong oxidation of oxygen-derived radicals, fewer byproducts such as one-ringed and two-ringed compounds are detected after absorption in hexane. Because of the generation of ozone, O, and OH radicals, the oxidative performance of these active species in the decomposition process is likely. First, owing to the relative higher concentration of oxygen, some of the oxygen molecules are dissociated by electron impact.

$$e + O_2 \rightarrow O(^3P) + O(^3P) + e \qquad (R13)$$

$$e + O_2 \rightarrow O(^1D) + O(^3P) + e \qquad (R14)$$
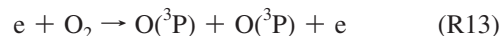
Additionally, some electrons can be attached by oxygen molecules,[48] which results in the lowest arc current in oxygen discharge compared with other kinds of gas discharge.

$$O_2 + M + e \rightarrow O_2^- + M \qquad (R15)$$
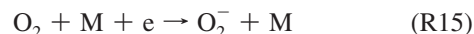
Naphthalene can directly react with oxygen exited states (O(^{3}P), O(^{1}D)), OH, and ozone through the following reactions:

$$C_{10}H_8 + O \rightarrow C_{10}H_7 + OH \qquad (R16)$$

$$C_{10}H_8 + O \rightarrow products \qquad (R17)$$

$$C_{10}H_8 + O_3 \rightarrow products \qquad (R18)$$

$$C_{10}H_8 + OH \rightarrow products \qquad (R19)$$

The reaction rate constant values are in the order of R19 (1 × 10^{-11} cm^3 molecule^{-1}s^{-1}) > R17 (2.44 × 10^{-13} cm^3 molecule^{-1} s^{-1}) > R16 (3 × 10^{-15} cm^3 molecule^{-1} s^{-1}) > R18 (3 × 10^{-19} cm^3 molecule^{-1} s^{-1}).[49–52] However, the highest rate constant is in R19, and the OH source is limited in the dry oxygen plasma. The rate constant of R16, one of the major OH generation processes, is about 1/1000 of that in R19. Naphthalene oxidation by ozone in destruction process seems insignificant for the lowest rate constant and easy dissociation, but it is very important for production of O radicals. Hence, this reaction channel between the O radical and naphthalene plays a vital role in the treatment. If the R16 produces enough OH radicals, R19 would be another important naphthalene oxidation channel.

NO and NO$_2$, as unfavorable gas phase products in an air discharge, can be identified by a FTIR spectrometer. It suggests that part of the energy in plasma is utilized for dissociation of nitrogen and oxygen, while some radicals do not react with naphthalene but are consumed to produce oxides of nitrogen. Some byproducts such as 1-nitronaphthalene and 2-nitroethenylbenzene in the hexane solvent are detected when air is used as the carrier gas. The presence of these two byproducts indicates reactions between NO, NO$_2$, and unstable intermediates. It is possible to ascribe the lower destruction rate with carrier gas of dry air to some parts of energetic electrons and radicals consumption by the reaction between nitrogen and oxygen. A simplified degradation pathway is proposed based on the qualitative analysis of products. The naphthalene destruction process is initialized through the reactions with oxygen-derived and nitrogen-derived radicals, and some intermediates are

formed. These intermediates consequently react with the O, OH, NO, and NO_2 active species and finally generate some stable products such as nitronaphthalene, CO_2, CO, and H_2O. The probable pathway includes all the reaction channels in nitrogen discharge and in oxygen discharge except for some reactions concerning the CN and HCN. Blin-Simiand et al. have investigated the species formation during the abatement of toluene by N_2/O_2 mixture discharge and reported that HCN and CN cannot be found for over 10% O_2.[42] Thereby reaction with nitrogen-derived radicals and oxidation by O radical play a dominant role in the degradation process in air discharge. 1-Nitronaphthalene and 2-nitroethenylbenzene are trace products in an air discharge, which indicate that reactions between some intermediates and NO and NO_2 take place in the destruction process. Whitehead et al.[11] and Kushner et al.[53] investigated the reactions between NOx and low carbon hydrocarbons such as C_3H_6 and C_3H_8 in the discharge by analyzing the kinetic data of these reactions. They found that NOx generated in the plasma can react with some hydrocarbon radicals. In this study, the reactions between NOx and intermediates can be proved by detecting the formation of NOx, nitrate, and nitrite products. But it is complicated to evaluate the contribution of NOx in the naphthalene destruction due to the lack of kinetic data for NOx interaction with higher carbon hydrocarbons ($C_6 \sim C_{10}$). On the other hand, it is known that NOx formation in discharge could consume part of the energy and free radicals, which can depress the target destruction process.

In the argon gliding arc, only two types of byproducts are detected by GC/MS due to less formation of free radicals. Electron collision plays the major role in the naphthalene destruction process. Possible destruction mechanisms in an Ar and an Ar/O_2 gliding arc discharges have been discussed.

4. Conclusion

In this study, the physical characteristics of the dc gliding arc plasma operated in different gases have been studied. The effects of different carrier gases, external resistances, and initial naphthalene concentrations on the plasma naphthalene destruction have also been investigated. The results show that average arc current increases in the order of oxygen < air < nitrogen < argon plasma, and the average arc voltage shows the reverse order. A maximum destruction rate of 92.3% can be achieved in the oxygen gliding arc with an external resistance of 50 kΩ. The highest treatment energy efficiency is about 3.6 g (kW h)$^{-1}$ in the oxygen discharge with external resistance of 93 kΩ, which can be attributed to the highest nonequilibrium degree in the plasma for this operating condition. Despite the destruction rate decline with rising naphthalene initial concentration, the degradation capacity still increases.

The poor naphthalene destruction in the argon discharge is caused by fewer radicals and its unsteadiness. Increasing oxygen concentration in the working gas can accelerate the decomposition process. Qualitative analysis of destructed products shows that reactions with the excited state of carrier gas molecules generated by electron dissociation are the key channels to initiate the decomposition process. The oxidation by oxygen-derived radicals plays a predominant role in the naphthalene treatment process in oxygen and air discharge. Additionally, reactions with CN and NOx radicals are observed in the nitrogen and air discharge, respectively.

References and Notes

(1) Keith, L. H.; Telliard, W. A. *Environ. Sci. Technol.* **1979**, *13*, 416.
(2) Finlayson Pitts, B. J.; Pitts, J. N. *Science* **1997**, *276*, 1045.
(3) Richter, H.; Howard, J. B. *Prog. Energy Combust. Sci.* **2000**, *26*, 565.
(4) Sharma, R. K.; Wooten, J. B.; Baliga, V. L.; Lin, X. H.; Chan, W. G.; Hajaligol, M. R. *Fuel* **2004**, *83*, 1469.
(5) Lair, A.; Ferronato, C.; Chovelon, J. M.; Herrrmann, J. M. *J. Photochem. Photobiol., A* **2008**, *193*, 193.
(6) Ania, C. O.; Cabal, B.; Arenillas, A.; Parra, J. B.; Rubiera, F.; Pis, J. J. *Water Res.* **2007**, *41*, 333.
(7) Mastral, A. M.; Garcia, T.; Callen, M. S.; Navarro, M. V.; Galban, J. *Environ. Sci. Technol.* **2001**, *35*, 2395.
(8) Ostapczuk, A.; Hakoda, T.; Shimada, A.; Kojima, T. *Plasma Chem. Plasma Process.* **2008**, *28*, 483.
(9) Shie, J. L.; Chang, C. Y.; Chen, J. H.; Tsai, W. T.; Chen, Y. H.; Chiou, C. S.; Chang, C. F. *Appl. Catal., B* **2005**, *58*, 289.
(10) Pramauro, E.; Prevot, A. B.; Vincenti, M.; Gamberini, R. *Chemosphere* **1998**, *36*, 1523.
(11) Demidyuk, V.; Hill, S. L.; Whitehead, J. C. *J. Phys. Chem. A* **2008**, *112*, 7862.
(12) Chen, H. L.; Lee, H. M.; Chen, S. H.; Chang, M. B.; Yu, S. J.; Li, S. N. *Environ. Sci. Technol.* **2009**, *43*, 2216.
(13) Oda, T. *J. Electrostat.* **2003**, *57*, 293.
(14) Urashima, K.; Chang, J. S. *IEEE Trans. Dielectrics Electrical Insulation* **2000**, *7*, 602.
(15) Fitzsimons, C.; Ismail, F.; Whitehead, J. C.; Wilman, J. J. *J. Phys. Chem. A* **2000**, *104*, 6032.
(16) Czernichowski, A. *Pure Appl. Chem.* **1994**, *66*, 1301.
(17) Fridman, A.; Nester, S.; Kennedy, L. A.; Saveliev, A.; Mutaf-Yardimci, O. *Prog. Energy Combust. Sci.* **1999**, *25*, 211.
(18) Mutaf-Yardimci, O.; Saveliev, A. V.; Fridman, A. A.; Kennedy, L. A. *J. Appl. Phys.* **2000**, *87*, 1632.
(19) Rueangjitt, N.; Sreethawong, T.; Chavadej, S. *Plasma Chem. Plasma Process.* **2008**, *28*, 49.
(20) Bo, Z.; Yan, J. H.; Li, X. D.; Chi, Y.; Cen, K. F. *Int. J. Hydrogen Energy* **2008**, *33*, 5545.
(21) Czernichowski, A. *Oil. Gas Sci. Technol.—Rev. Inst. Franc. Petrol.* **2001**, *56*, 181.
(22) Bo, Z.; Yan, J. H.; Li, X. D.; Chi, Y.; Cen, K. F. *J. Zhejiang Univ.—Sci. A* **2008**, *9*, 695.
(23) Bo, Z.; Yan, J.; Li, X.; Chi, Y.; Cen, K. *J. Hazard. Mater.* **2008**, *155*, 494.
(24) Indarto, A.; Choi, J. W.; Lee, H.; Song, H. K. *Environ. Chem. Lett.* **2008**, *6*, 215.
(25) Krawczyk, K.; Ulejczyk, B. *Plasma Chem. Plasma Process.* **2004**, *24*, 155.
(26) Yan, J. H.; Liu, Y. N.; Bo, Z.; Li, X. D.; Cen, K. F. *J. Hazard. Mater.* **2008**, *157*, 441.
(27) Yu, L.; Yan, J. H.; Tu, X.; Li, X. D.; Lu, S. Y.; Cen, K. F. *Europhys. Lett.* **2008**, *83*, 45001.
(28) Benstaali, B.; Moussa, D.; Addou, A.; Brisset, J. L. *Eur. Phys. J.—Appl.Phys.* **1998**, *4*, 171.
(29) Moussa, D.; Abdelmalek, F.; Benstaali, B.; Addou, A.; Hnatiuc, E.; Brisset, J. L. *Eur. Phys. J.—Appl.Phys.* **2005**, *29*, 189.
(30) Locke, B. R.; Sato, M.; Sunka, P.; Hoffmann, M. R.; Chang, J. S. *Ind. Eng. Chem. Res.* **2006**, *45*, 882.
(31) Tu, X.; Yu, L.; Yan, J. H.; Cen, K. F.; Cheron, B. G. *Phys. Plasmas* **2009**, *16*, 113506.
(32) Ito, Y.; Shiki, H.; Takikawa, H.; Ootsuka, T.; Okawa, T.; Yamanaka, S.; Usuki, E. *Jpn. J. Appl. Phys.* **2008**, *47*, 6956.
(33) Du, C. M.; Yan, J. H.; Li, X. D.; Cheron, B. G.; You, X. F.; Chi, Y.; Ni, M. J.; Cen, K. F. *Plasma Chem. Plasma Process.* **2006**, *26*, 517.
(34) Das, A. K. *Arc root dynamics in high power plasma torches—Evidence of chaotic behavior*; 14th Natioal Symposium on Plasma Science and Technology (Plasma-99), 1999, Amritsar, India.
(35) Richard, F.; Cormier, J. M.; Pellerin, S.; Chapelle, J. *J. Appl. Phys.* **1996**, *79*, 2245.
(36) Czernichowski, A.; Nassar, H.; Ranaivosoloarimanana, A.; Fridman, A. A.; Simek, M.; Musiol, K.; Pawelec, E.; Dittrichova, L. *Acta Phys. Pol., A* **1996**, *89*, 595.
(37) Mutaf-Yardimci, O.; Saveliev, A. V.; Porshnev, P. I.; Fridman, A. A.; Kennedy, L. A. *Heat Mass Transfer Plasma Cond.* **1999**, *891*, 304.
(38) Nair, S. A.; Pemen, A. J. M.; Yan, K.; van Gompel, F. M.; van Leuken, H. E. M.; van Heesch, E. J. M.; Ptasinski, K. J.; Drinkenburg, A. A. H. *Fuel Process. Technol.* **2003**, *84*, 161.

(39) Kim, H. H.; Kobara, H.; Ogata, A.; Futamura, S. *IEEE Trans. Ind. Appl.* **2005**, *41*, 206.

(40) Herron, J. T. *Plasma Chem. Plasma Process.* **2001**, *21*, 581.

(41) Rousseau, A.; Gatilova, L. V.; Ropcke, J.; Meshchanov, A. V.; Ionikh, Y. Z. *Appl. Phys. Lett.* **2005**, 86.

(42) Blin-Simiand, N.; Jorand, F.; Magne, L.; Pasquiers, S.; Postel, C.; Vacher, J. R. *Plasma Chem. Plasma Process.* **2008**, *28*, 429.

(43) Liu, J. H.; Xiao, Q. M.; Wang, L. P.; Yao, Z.; Ding, H. B. *Plasma Sci. Technol.* **2009**, *11*, 171.

(44) Yea, Z. L.; Zhang, Y. N.; Li, P.; Yang, L. Y.; Zhang, R. X.; Hou, H. Q. *J. Hazard. Mater.* **2008**, *156*, 356.

(45) Delair, L.; Brisset, J. L.; Cheron, B. G. *High Temp. Mater. Process.* **2001**, *5*, 381.

(46) Becker, K. H.; Engelhardt, B.; Geiger, H.; Kurtenbach, R.; Schrey, G.; Wiesen, P. *Chem. Phys. Lett.* **1992**, *195*, 322.

(47) Brownsword, R. A.; Gatenby, S. D.; Herbert, L. B.; Smith, I. W. M.; Stewart, D. W. A.; Symonds, A. C. *J. Chem. Soc., Faraday Trans.* **1996**, *92*, 723.

(48) McDaniel, E. W. *Collision Phenomena in Ionized Gases*; Wiley: New York, 1964.

(49) Roger Atkinson, S. M. A. *Int. J. Chem. Kinet.* **1986**, *18*, 569.

(50) Frerichs, H.; Tappe, M.; Wagner, H. G. *Ber. Bunsenges. Phys. Chem.* **1990**, *94*, 658.

(51) Mati, K.; Ristori, A.; Pengloan, G.; Dagaut, P. *Combust. Sci. Technol.* **2007**, *179*, 1261.

(52) Atkinson, R. *Chem. Rev.* **1986**, *86*, 69.

(53) Dorai, R.; Kushner, M. J. *J. Phys. D: Appl. Phys.* **2001**, *34*, 574.